

Article

Catalytic Performance of Ag₂O and Ag Doped CeO₂ Prepared by Atomic Layer Deposition for Diesel Soot Oxidation

Tatiana V. Ivanova ^{1,*}, Tomáš Homola ² , Anton Bryukvin ¹ and David C. Cameron ² 

¹ ASTRaL Team, Laboratory of Green Chemistry, School of Engineering Science, Lappeenranta University of Technology, Sammonkatu 12, FI-50130 Mikkeli, Finland; bryukvin@gmail.com

² R & D Centre for Low-Cost Plasma and Nanotechnology Surface Modification, Masaryk University, Kotlářská 267/2, 611 37 Brno, Czech Republic; tomas.homola@mail.muni.cz (T.H.); dccameron@mail.muni.cz (D.C.C.)

* Correspondence: tatiana.ivanova@student.lut.fi; Tel.: +358-401-978-567

Received: 31 May 2018; Accepted: 28 June 2018; Published: 4 July 2018



Abstract: The catalytic behaviour of Ag₂O and Ag doped CeO₂ thin films, deposited by atomic layer deposition (ALD), was investigated for diesel soot oxidation. The silver oxide was deposited from pulses of the organometallic precursor (hfac)Ag(PMe₃) and ozone at 200 °C with growth rate of 0.28 Å/cycle. Thickness, crystallinity, elemental composition, and morphology of the Ag₂O and Ag doped CeO₂ films deposited on Si (100) were characterized by ellipsometry, X-ray diffraction (XRD), X-ray photoelectron spectroscopy (XPS), atomic force microscopy (AFM), and field emission scanning electron microscopy (FESEM), respectively. The catalytic effect on diesel soot combustion of pure Ag₂O, CeO₂, and Ag doped CeO₂ films grown on stainless steel foil supports was measured with oxidation tests. Nominally CeO₂:Ag 10:1 doped CeO₂ films were most effective and oxidized 100% of soot at 390 °C, while the Ag₂O films were 100% effective at 410 °C. The doped films also showed much higher stability; their performance remained stable after five tests with only a 10% initial reduction in efficiency whereas the performance of the Ag₂O films reduced by 50% after the first test. It was concluded that the presence of Ag⁺ sites on the catalyst is responsible for the high soot oxidation activity.

Keywords: silver oxide; cerium oxide; oxidation; diesel soot; catalysis; ALD

1. Introduction

The number of diesel-powered vehicles has increased rapidly in recent years due to their reduced fuel consumption and thus lower CO₂ emission compared to petrol engines. However, diesel engines produce a high content of nitrogen oxides (NO_x) and particulate matter (PM) in their exhaust [1]. These emissions have a negative impact on human health causing respiratory, cardiovascular, and lung diseases, as well as on the environment such as disruption of the natural growth of plants and pollution of air, water, and soil [2,3]. Even though it is likely that many diesel engines will be replaced by petrol or electric engines in the future, there will still be a great need for diesel exhaust cleaning for some time to come.

In order to remove soot from the exhaust, diesel particulate filters (DPFs) are widely used [1]. Conventional DPFs require periodic regeneration by increasing the temperature of the exhaust gases to the soot combustion temperature, which is approximately 600 °C [4]. This method results in an increase in fuel consumption and clogging of the DPF by ash resulting in a slow increase of back pressure in the exhaust [1].

The composition of the exhaust mixture also affects the catalytic activity. Oxygen and NO₂ are generally used to oxidize diesel soot. NO contained in the raw exhaust gas is oxidized with excess oxygen into NO₂. Therefore, the development of catalysts, which can produce highly reactive oxygen species from O₂ molecules and NO₂ from NO, is the key issue. The catalyst promotes NO to NO₂ oxidation and NO₂ is then transported via the gas phase over the soot particles, oxidizing carbon while being reduced back to NO [5,6].

The preferred solution for continuous regeneration of the DPF is a catalysed diesel particulate filter (C-DPF) [7]. The main requirements for the catalyst are a reduction in temperature at which soot combustion occurs and long-term thermal and chemical stability.

Ceria-based catalysts have been studied in depth for various environmental applications such as three-way catalysts (TWC) for automotive pollution control, fluid catalytic cracking (FCC), and fuel cells [8,9]. The high potential of ceria as a catalyst is due to its fast and reversible reduction to sub-stoichiometric phases (CeO₂-CeO_{2-x}) as well as the high mobility of oxygen ions in its crystal lattice [10]. However, the use of metal-doped oxide catalysts can improve the performance of the bare oxide due to the increased mobility of oxygen species or the facilitation of the redox mechanisms associated with oxygen release/adsorption [11].

The influence of doping elements on the catalytic properties of ceria has been reported on recently by many researchers. The catalytic activity of ceria can be enhanced by doping with isovalent (Ti⁴⁺, Zr⁴⁺, Hf⁴⁺, Sn⁴⁺, etc.) and aliovalent (Zn²⁺, La³⁺, Ag⁺, Eu³⁺, etc.) cations into the ceria lattice [12–15]. Furthermore, the beneficial influence of Rh, Pd, Cu, Au, and Ag supported CeO₂ catalysts has been reported on elsewhere [16–18]. These reports showed increased electron mobility between the cerium buffer layer and support, favouring the formation of oxygen vacancies in CeO₂. Rangaswamy et al. [19] studied CeO₂-Sm₂O₃ and CeO₂-La₂O₃ catalysts, which could oxidize 50% of diesel soot under loose contact mode at 517 and 579 °C, respectively.

Among the metal additives investigated so far, Ag-based materials are the most promising catalysts for oxidizing diesel soot at low temperatures. Aneggi et al. [20] reported the effect of Ag addition on various metal oxides (CeO₂, ZrO₂, Al₂O₃) during soot oxidation activity. They showed that Ag/CeO₂ and Ag/ZrO₂ catalysts have high soot oxidation activity in the temperature region around 300 °C under tight contact mode. Haneda et al. [21] also performed isotopic transient kinetic analysis on Ag/ZrO₂ catalyst and concluded that the presence of Ag⁺ sites in Ag/ZrO₂ was responsible for the high soot oxidation activity. Ag and Fe doped Mn₂O₃ catalysts were examined by Kuwahara et al. to enhance soot oxidation under tight contact mode and showed the T50 (the temperature for 50% of soot combustion) at 290 °C and at 328 °C, respectively. Based on their measurements, the mechanism of soot oxidation was proposed to be by the activated lattice oxygen species in Ag doped Mn₂O₃ catalyst via the redox of Ag⁰/Ag₂O species [22].

Machida et al. [9] investigated silver loading onto CeO₂ and showed the enhancement of catalytic activity for soot oxidation because of the enhanced generation of superoxide. Shimizu et al. [23] showed that the presence of Ag metal nanoparticles on CeO₂ significantly improved the reactivity of CeO₂ lattice oxygen during soot decomposition under oxygen and under inert atmosphere. In addition, a dopant of silver in CeO₂ may increase oxygen mobility due to a weakened Ce–O bond [24].

There are a number of methods of preparation of Ag doped CeO₂ catalysts such as co-precipitation [25], impregnation [19,26], and liquid-phase chemical reduction [20]. We chose to use atomic layer deposition (ALD). The benefits of ALD compared to the other methods are extreme film thickness uniformity, precise thickness control, excellent step coverage, and high reproducibility. The thickness of the films can be easily controlled by controlling the number of deposition cycles. Furthermore, the fact that ALD operates via self-limiting surface reactions in consecutive cycles means that doping materials can be introduced with greater control and tuning than other deposition methods. ALD can be used to deposit catalytic coatings on high surface area porous powder supports or on geometrically complex structures [27] such as particulate filters in diesel engine exhaust systems.

In this study, we investigated the ALD of Ag₂O and Ag doped CeO₂ for catalytic applications in soot combustion under loose contact mode. The crystal structure, morphology, and composition properties of the deposited films were analysed. The effect of doping on the efficacy of soot combustion in annealing tests was also studied, paying particular attention to the doping concentration and oxidation state of silver in the CeO₂ thin films.

2. Materials and Methods

2.1. Catalyst Preparation

The deposition of Ag doped cerium oxide was carried out using an F-120 ALD reactor (ASM Microchemistry Ltd., Espoo, Finland). Thin films were deposited with different doping concentrations at a reaction temperature of 200 °C. The cyclic nature of ALD means that pulses of dopant can easily be incorporated into the main process. The desired composition of catalytic thin film can be achieved by depositing n cycles of the base CeO₂ material (where n can be varied to suit the required doping level) with one cycle of the doping material inserted (Figure 1). The supercycle ($n + 1$), which consists of two individual ALD processes, was repeated x times until the required film thickness was achieved. The process for CeO₂-based material contains two half-cycles using 2,2,6,6-tetramethyl-3,5-heptadionatecerium Ce(C₁₁H₁₉O₂)₄ (Ce(thd)₄ for brevity) and O₃ as precursors. The Ag doping material also comprises two half-cycles of Ag precursor (see below) and O₃.

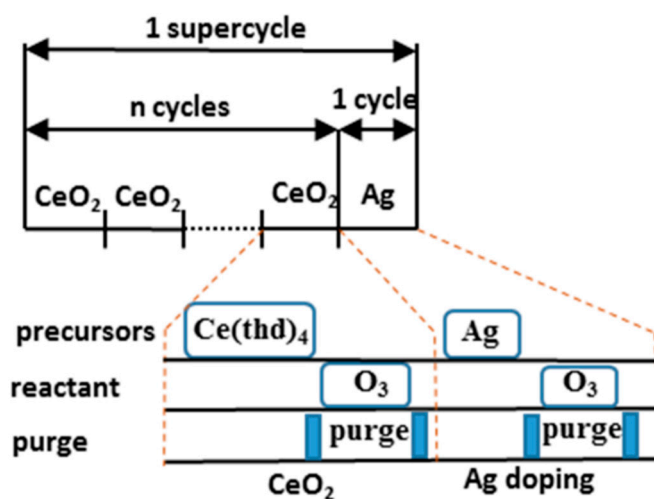


Figure 1. A schematic representation of the atomic layer deposition (ALD) supercycle used to deposit Ag doped CeO₂ catalytic thin films.

Ce(thd)₄ (Volatec, Porvoo, Finland) and trimethylphosphine (hexafluoroacetylacetonato)-silver Ag(CF₃COCHCOF₃)P(CH₃)₃ ((hfac)Ag(PMe₃), 99%; Strem Chemicals, Newburyport, MA, USA) were used as Ce and Ag precursors respectively. Ozone O₃ was used as the co-reactant in both cases and was generated by an ozone generator (Wedeco Modular 4HC Lab, Herford, Germany) from a pure oxygen (>99.999%) source. Ozone concentration was 120 g/m³. Nitrogen (>99.999%) was used as a carrier and purge gas between precursor pulses. The pressure in the reactor was approximately 1 mbar. Ce(thd)₄ and (hfac)Ag(PMe₃) were evaporated at 160 and 80 °C, respectively to achieve sufficient vapour pressure. The saturated deposition rate in the ALD supercycle should be obtained when the two individual ALD processes are in saturation. We used the previously optimized CeO₂ ALD process parameters: 1.5 s Ce(thd)₄ dose, 2.5 s purge, 2.5 s O₃ dose, 2.5 s purge [28]. The pulse time for (hfac)Ag(PMe₃) was varied from 0.5 to 4 s in 0.5 s steps while keeping the O₃ pulse time constant at 2.5 s. After finding the optimal pulse time for (hfac)Ag(PMe₃) the pulse time for O₃ was determined with the same method with 2.5 s of the purge time.

In order to achieve doping of CeO₂ with Ag, one supercycle consisted of n CeO₂ cycles, with n equal to 10, 20, and 30, and 1 cycle of Ag. The supercycle was repeated 150, 75, and 50 times for CeO₂:Ag ratios 10:1, 20:1, and 30:1 respectively in order to achieve comparable film thicknesses.

Silicon substrates <100> (Si-Mat, Kaufering, Germany) were used for process development while stainless steel foil AISI 316 with a thickness of 0.025 mm (Goodfellow Cambridge Ltd., London, UK) was used as a substrate for soot burning tests. Stainless steel foil was chosen because of its relatively low weight, which reduced the error during weighing of samples to determine the amount of soot oxidation. The substrates were cut in pieces of 20 mm × 10 mm and cleaned using an ultrasonic bath with acetone, isopropanol, and deionized water consecutively, each with a time of 5 min and thereafter dried using compressed air.

2.2. Soot Deposition System

The soot deposition system was described in detail in the previous report [28]. Briefly, the diesel soot was generated with a Webasto diesel engine preheater (Webasto group, Stockdorf, Germany) from diesel fuel and air. The samples were placed on the heating plate and exposed to exhaust gases for 1.5 min. The amount of deposited soot was measured by weighing the samples.

2.3. Catalyst Characterization

A spectroscopic ellipsometer J.A. Woollam M-2000UI (J.A. Woollam Co., Lincoln, NE, USA) was used to determine the catalytic film thickness. This was obtained by using a Cauchy model for fitting.

The surface topography of the catalytic thin films was evaluated with field emission scanning electron microscopy (FESEM) Hitachi S-4800 (Hitachi, Tokyo, Japan). An atomic force microscopy (AFM) (Park NX10, Park Systems, Suwon, Korea) was utilized for analysing the film morphological properties such as roughness and cluster size. All measurements were done in non-contact mode with a cantilever force constant of 42 N/m.

The crystal structure of the catalytic materials was studied by a Rigaku SmartLab[®] Type F XRD (Rigaku, Tokyo, Japan; Cu-K α radiation, $\lambda = 1.5418 \text{ \AA}$). The grazing incidence X-ray diffraction (GIXRD) scan was collected with a grazing incidence angle of 0.5°. Scan speed of 0.9°/min and 2 θ values from 20° to 90° were used. The high resolution scan was taken with speed 0.045°/min.

The surface chemical composition, bonding properties and analysis of impurities in the deposited films were investigated by X-ray photoelectron spectroscopy (XPS) using an ESCALAB 250Xi (Thermo Scientific, Loughborough, UK) with a monochromated Al-K α (energy of 1486.7 eV) X-ray source in the constant pass energy mode with a value of 50 eV. For high resolution spectra of Ag 3d a pass energy of 20 eV with resolution 0.1 eV was used. Charging compensation by an electron flood source was used in all measurements to minimize binding energy shifts. The binding energy of C 1s was set to be 284.5 eV as an internal standard for calibration. Sputtering by Ar⁺ ions at 2 kV for 20 s was applied to remove surface contaminations and obtain actual carbon levels in the films. Deconvolution and fitting of the obtained peaks were made with Avantage software (Version 5.938) using Smart type background and applying 90:10 Gaussian-Lorentzian peaks.

2.4. Catalytic Activity

Five samples of Ag doped CeO₂, pure CeO₂ and pure Ag₂O catalytic coatings were separately deposited on stainless steel foils for evaluation of catalytic activity. For measurement of the amount of combusted soot, annealing tests were performed by placing the catalytic samples covered with soot into an oven and measuring the weight loss of the samples over 2 h in the temperature range of 300–490 °C in ambient atmosphere. The molar ratio of catalysts to carbon was approximately 1:80 with average soot mass of 0.7 g. The annealing measurements were repeated 5 times to evaluate reproducibility of the prepared catalysts.

3. Results and Discussion

3.1. Ag_2O and Ag-Doped CeO_2 ALD Film Deposition

3.1.1. Ag_2O

The concept of the supercycle can be effective when two individual processes are compatible with each other and each is in saturation. Therefore, before the introduction of Ag as a dopant into the CeO_2 structure, silver oxide thin films were deposited first on silicon substrates to find the self-limiting growth regime of the ALD process. This could be assessed by measuring the growth rate as a function of the amount of precursor delivered into the reactor. The ALD saturation growth study was carried out at deposition temperature of 200 °C. This temperature was chosen to match the reaction temperature of CeO_2 and it has been shown that the nucleation period of Ag is significantly shortened at this temperature [29]. Figure 2 shows the saturation curves for (hfac)Ag(PMe₃) and O₃. The pulsing time of (hfac)Ag(PMe₃) or O₃ was adjusted within the range of 0.5–4 s while the other precursor pulse was fixed at 2.5 s. The saturation of (hfac)Ag(PMe₃) and O₃ precursors can be seen at 2.5 s with constant Ag_2O growth rate of 0.28 Å/cycle. No further increase of the growth rate was noticed after increasing the precursor pulse time up to 4 s.

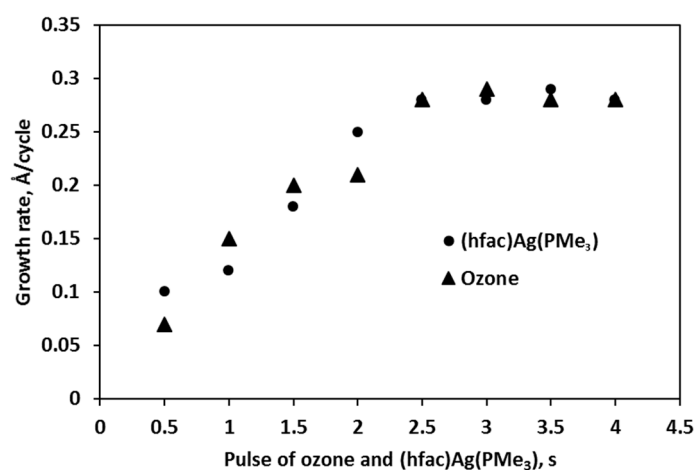


Figure 2. The effect of ozone and (hfac)Ag(PMe₃) pulse time on the growth rate of silver oxide at 200 °C reactor temperature.

Figure 3 shows the Ag_2O film thickness versus the number of ALD cycles from 10 to 750 deposited at 200 °C. From Figure 3 it can be seen that the thickness increases linearly after 100 ALD cycles. The incorporation of silver atoms is directly related to the density of hydroxyl groups on the substrate surface that act as adsorption sites for (hfac)Ag(PMe₃) molecules. As illustrated in Figure 3, the initial growth rate of the films per cycle (GPC) is substrate dependent at the start of the ALD process and it takes about 100 cycles to obtain a stable GPC of 0.28 Å/cycle. The film growth can be separated into two regimes: an island-like growth for the first 100 cycles and layer-by-layer growth as is expected from the proceeding atomic layer deposition. If the bare Si has a higher density of reactive sites compared to the deposited Ag_2O or these sites have a higher reactivity than the reactive sites on Ag_2O , then the growth rate will initially be higher until a complete film is formed. Alternatively, some hfac ligands may not be completely removed by ozone and may remain bound to the surface. These comments are expanded on in Section 3.1.2.

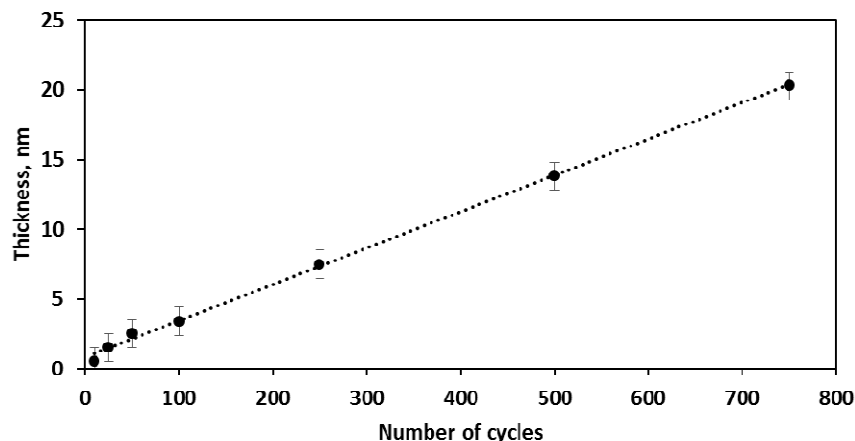


Figure 3. Thickness of the silver oxide film as a function of the number of deposition cycles at the deposition temperature of 200 °C.

3.1.2. Ag Doped CeO₂

The film thickness after deposition with different CeO₂:Ag ratios was measured by spectroscopic ellipsometry. The total number of CeO₂ cycles was chosen to be 1500 while the number of Ag cycles was varied from 50 up to 150 according to the supercycle configuration. Growth rate of the films per cycle (GPC) over the total number of ALD cycles is shown in Figure 4 as a function of Ag dopant fraction in CeO₂ film. The reduction of GPC with increasing Ag dose observed in Figure 4 could be the result of a slight etching of CeO₂ by (hfac)Ag(PMe₃), but it could also be due to nucleation delay and the inhibition of CeO₂ growth after (hfac)Ag(PMe₃) pulsing.

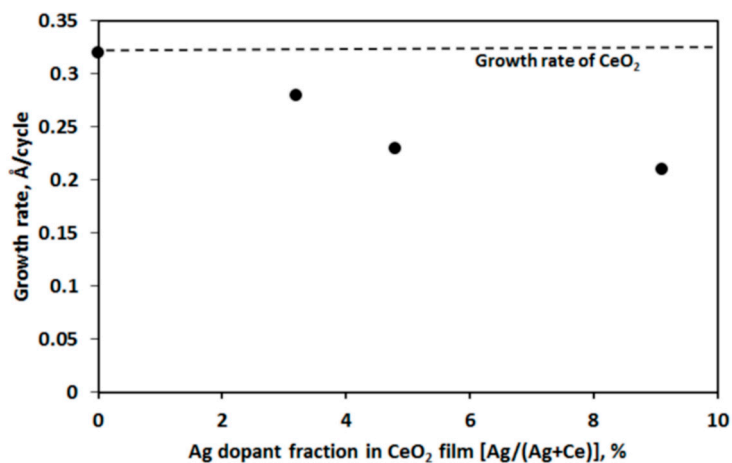


Figure 4. The effect of Ag concentration on the growth rate of Ag doped CeO₂ thin films at 200 °C reactor temperature.

The comparison of the two calculated and experimental silver doping concentrations inside the Ag doped CeO₂ films is shown in Figure 5. The calculated value is determined by the ratio of the number of doping ALD cycles divided by the total number of ALD cycles in one supercycle ($1/(n + 1)$). The experimental value is obtained from XPS measurements. It is worth emphasizing that the concentrations of dopant do not relate directly to the doping efficiency. Some of the dopant silver atoms might have formed silver oxide or alloy clusters rather than only doping the film, as will be discussed in Section 3.2.

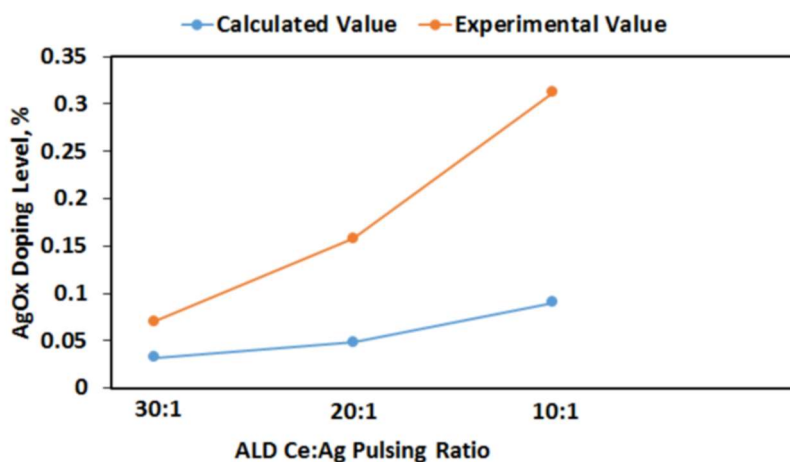


Figure 5. Relationship between CeO₂:Ag pulsing ratio vs. silver molar percent in the corresponding Ag doped CeO₂ thin films.

The hypothetical deposition of Ag doped CeO₂ by ALD can be explained as follows: (a) Ce(thd)₄ adsorbs on nucleation sites (–OH) and dissociates into the attached fraction Ce(thd)_x*, where * designates surface species, with *x* varying from 1 to 3 depending on the number of OH sites it bonds to. Most probably, some –OH groups remain unreacted, due to steric hindrance; (b) Ozone regenerates O* groups which can act as nucleation sites during subsequent (hfac)Ag(PMe₃) exposures. The O₃ half-cycle also probably results in the formation of OH groups because of decomposition of the precursor ligand; (c) (hfac)Ag(PMe₃) may adsorb on Ce–O* or Ce–OH nucleation sites and on unreacted –OH groups, and dissociates into Ce(hfac)* and Ag(hfac)* species; (d) ozone may react with Ce(hfac)* and Ag(hfac)* species regenerating O* groups for further Ce(thd)₄ exposures. We propose that during Ce(thd)₄ treatments, not all –OH or regenerated O* groups can react with the precursor or, as mentioned above, hfac ligands remain bound to the surface and cannot be completely removed by ozone. This statement is supported by XPS measurements, where a high level of impurities was noticed, and is discussed in detail in Section 3.2. It could be the reason for formation of Ag₂O clusters in the films with higher concentration of Ag doping, as will be considered during AFM and SEM analysis. With more CeO₂ ALD cycles, more nucleation sites are generated and this facilitates the growth of CeO₂ thin film with Ag as a dopant.

3.2. Catalyst Characterization

Ag₂O and Ag-Doped CeO₂

In examining the nucleation effect and morphology of the resulting ALD of Ag₂O, several AFM images were taken with variable ALD cycles (Figure 6). The average size of Ag₂O nanoparticles after 25 ALD cycles was around 22 nm with film roughness of 1.5 nm. After 100 ALD cycles, large nanoparticles with size of around 40 nm were present with a high nanoparticle density (Figure 6a) and overall surface coverage. The AFM image of 500 cycles of Ag₂O film is shown in Figure 6b, which demonstrates that the surface is now fully covered with silver, having grain sizes between 40 and 46 nm. As was shown in Figure 3, the nucleation region for Ag₂O ALD occurs over 100 cycles; Ag₂O films can nucleate and grow by the Volmer–Weber (VW) growth mechanism, where the deposited atoms form islands or clusters and three dimensional aggregates on the substrate. Growth of these clusters, along with coarsening, can be a cause of rough thin films on the substrate surface [30].

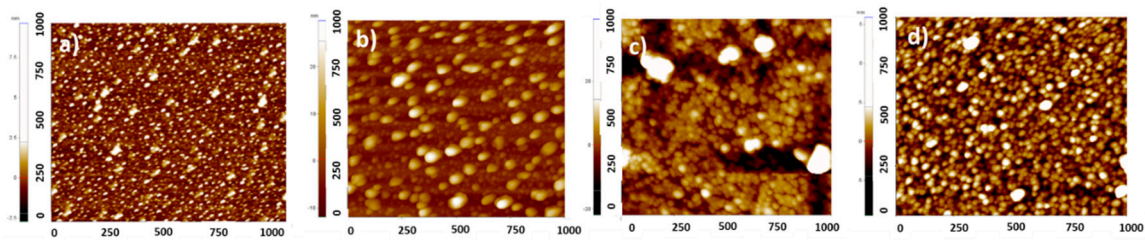


Figure 6. The atomic force microscopy (AFM) non-contact mode images of Ag_2O deposited with: (a) 25 cycles (R_a 0.7 nm); (b) 100 cycles (R_a 1.5 nm); (c) 250 cycles (R_a 1.6 nm); and (d) 500 cycles (R_a 1.7 nm). Axis scales are in nm.

All the Ag_2O thin films deposited on Si had a visual matt finish, which is a sign of rough microstructure. SEM studies supported the AFM results (Figure 7). The 250 and 500 ALD cycles films were confirmed to consist of particles with widely different sizes as a result of coalescence and secondary nucleation on existing particles.

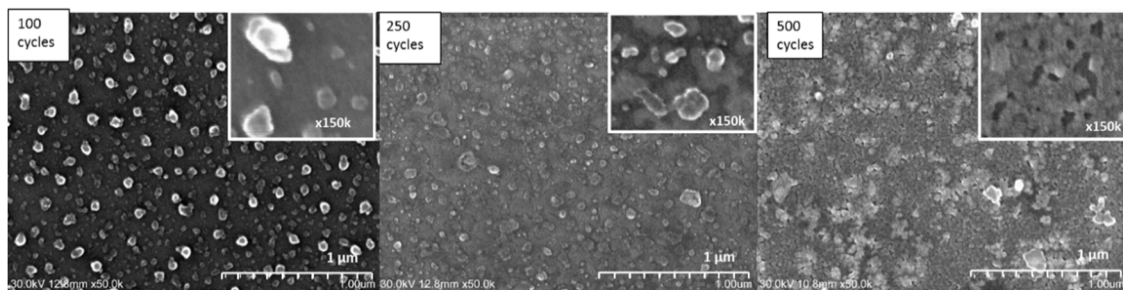


Figure 7. Scanning electron microscope (SEM) images of Ag_2O thin films deposited with different number of cycles at 200 °C resulting in different thicknesses (5.8, 8.8, and 13.8 nm).

The AFM and SEM analyses on Figures 8 and 9 show that the surface morphology of Ag doped CeO_2 films changes in accordance with silver concentration in the film. It can be seen that the reduction of Ag concentration dramatically decreases crystal and cluster sizes in doped films. Figures 8a and 9a suggest that higher concentration of Ag ($\text{CeO}_2:\text{Ag}$ 10:1) inhibits CeO_2 growth so that the Ag nuclei are not covered with CeO_2 and so the next Ag cycle nucleates more easily on top of the Ag and can therefore form bigger crystals of about 50 nm in size. Such large nanoparticles were noticed on pure Ag_2O and described above. With lower doping concentration of Ag in CeO_2 thin films, no crystals larger than 25 nm were noticed.

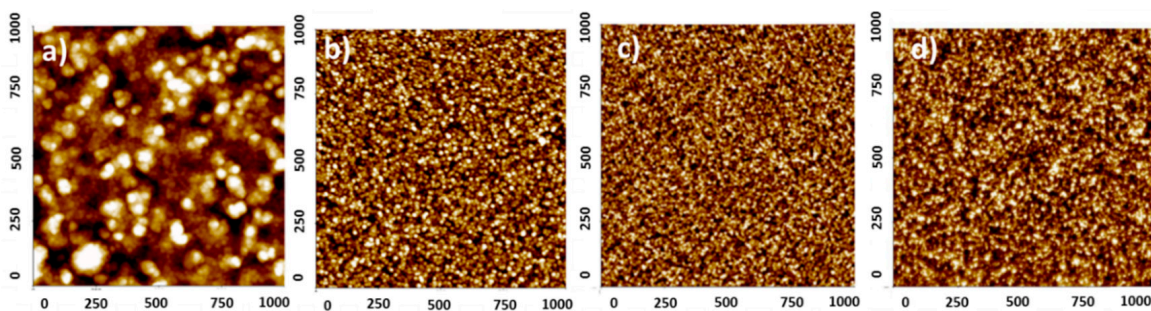


Figure 8. The AFM non-contact mode images of Ag doped CeO_2 in different $\text{CeO}_2:\text{Ag}$ ratios deposited at 200 °C: (a) 10:1; (b) 20:1; (c) 30:1; and (d) CeO_2 . The scales are in nm.

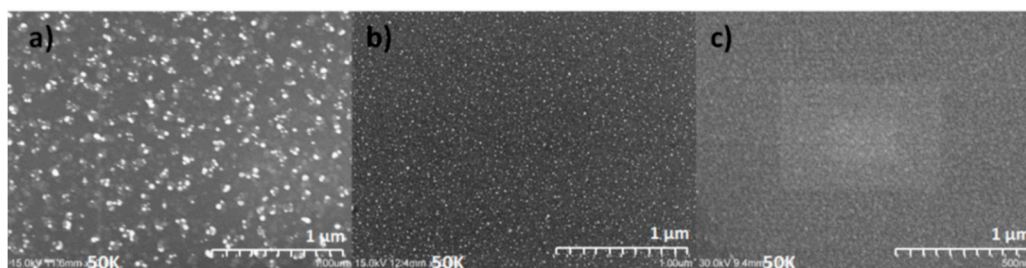


Figure 9. SEM of Ag doped CeO₂ in different CeO₂:Ag ratios (a) 10:1, (b) 20:1, and (c) 30:1 deposited at 200 °C.

Figure 10a shows XRD spectra of Ag₂O, CeO₂, and Ce:Ag 10:1, 20:1, and 30:1 Ag doped CeO₂ films in the 2θ range of 20°–90°. The Ag₂O films showed strong X-ray diffraction peaks at 2θ = 32.7° and 38.3° related to the (111) and to (200) cubic planes of Ag₂O, respectively (ICCD Card No: 00-41-1104). They revealed that the films deposited at 200 °C contained only Ag₂O crystallites. The diffraction peaks at 2θ angles of 28.6°, 33.6°, 47.6°, and 56.3° can be identified for all the other samples and attributed to (111), (200), (220), and (311) planes of cubic cerium oxide, respectively (COD database, card No 9009008). The XRD patterns of CeO₂, Ag₂O, and Ag doped CeO₂ in the 2θ range 24–40° were expanded (Figure 10b) to analyse the position of CeO₂ and Ag₂O reflections in the X-ray spectra in more detail. Figure 10b shows that the cerium oxide peak intensity and the shape of (200) plane reflection in the Ag doped CeO₂ samples decreased and broadened, respectively, with increasing Ag doping, compared to the pure CeO₂ catalyst.

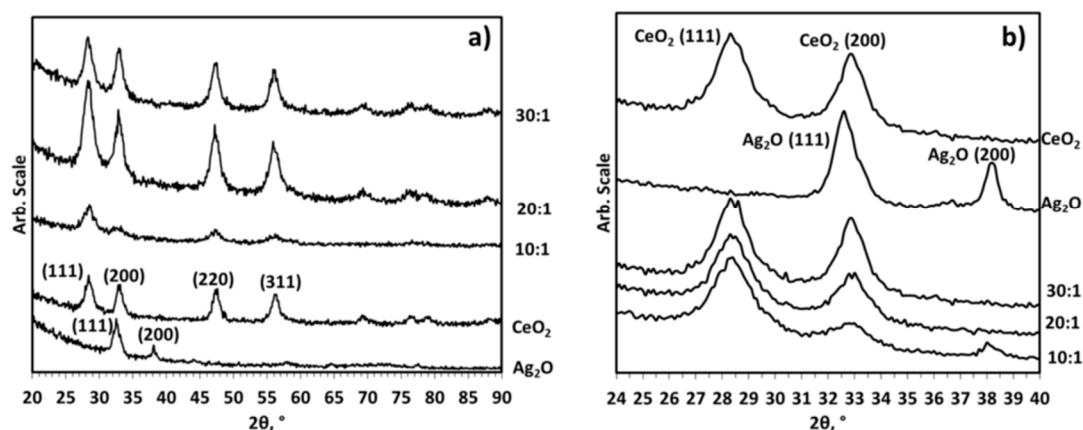


Figure 10. (a) X-ray diffraction (XRD) patterns of Ag₂O, CeO₂ and Ag doped CeO₂ with different Ce:Ag ratios 10:1, 20:1, and 30:1 deposited at 200 °C. (b) XRD patterns of slow scans of CeO₂, Ag₂O and Ag doped CeO₂ with different Ce:Ag ratios 10:1, 20:1, 30:1 in the 2θ range of 24–40°.

The mean grain size, assuming spherical grains, of CeO₂ can be determined from the full width at half maximum (FWHM) of the (111) XRD peak, through Scherrer's equation. The grain sizes calculated from the (111) plane reflection of CeO₂ are indicated in Table 1. XRD analyses confirm the decrease of the CeO₂ crystallite size of (111) plane as the Ag amount increases. This behaviour is related to the occurrence of lattice defects due to the presence of the dopant, which leads to deformations in the crystalline structure and smaller crystallites. The XRD data do not show any peaks related to Ag species for CeO₂:Ag 20:1 and 30:1 catalysts, which is, most probably, demonstrative of a high distribution of the dopants in the CeO₂ samples. The CeO₂ (200) and Ag₂O (111) appear at very similar positions. However, for higher amount of Ag doping Ce:Ag 10:1, a small peak from the Ag₂O (200) plane reflection can be observed (Figure 10b). In the CeO₂ lattice, the radius of Ce⁴⁺ ion is 0.97 Å. However, the ionic radius of Ag⁺ ions is 1.28 Å [31]. As such, substitution or replacement of Ag⁺ ions

for Ce^{4+} ions in the CeO_2 lattice requires high energy [32] and from the XRD there is no evidence of significant substitutional doping during ALD of Ag doped CeO_2 thin films from a shift in the position of the CeO_2 peaks to smaller angles. Ag_2O forms as metal oxide or alloy clusters in CeO_2 :Ag 10:1 catalyst and inhibits CeO_2 crystal formation.

Table 1. Grain size of CeO_2 (111) plane reflection based on Scherrer's equation.

Catalyst	Grain Size of CeO_2 (111) (nm)
CeO_2	10.2
Ce:Ag 30:1	8.7
Ce:Ag 20:1	7.1
Ce:Ag 10:1	6.2

XPS was employed to analyse the chemical state of the as-deposited Ag_2O thin films and the Ag doping in CeO_2 films, which were controlled by varying the Ce:Ag supercycle binary process pulse ratio. The information on silver and cerium oxidation states was obtained from the high resolution Ag 3d and Ce 3d spectra after Ar^+ bombardment to exclude surface contaminations.

Using the values of surface atomic composition from Table 2, an estimation of the O/Ce and O/Ag atomic ratio can be obtained. The ratio O/Ce for the cerium oxide deposited at 200 °C is around two, which indicates that the pure CeO_2 is stoichiometric. The carbon impurity level is around 21 at.%, which arise from the $\text{Ce}(\text{thd})_4$. The Ag to O ratio in the Ag_2O films was estimated to be close to 2:1, which indicates that the film primarily consists of Ag_2O with 14.2% of carbon, 0.5% of F, and 3% of N as the main impurities in that film. With regard to the Ag/Ce surface atomic ratio, an important enhancement with Ag loading is observed, indicative of an increase in the number of Ag surface atoms. We found from survey spectra that by changing the Ce:Ag ratio from 30:1 to 10:1 the amount of Ag increases from ~2 at.% to ~9.7 at.%, as measured by XPS (Table 2).

Table 2. Surface elemental composition of Ag doped CeO_2 , Ag_2O , and CeO_2 thin films.

Catalyst	Surface Composition (at.%)						Ag/Ce (from Survey)
	Ce 3d	Ag 3d	O 1s	C 1s	F 1s	N 1s	
Ce:Ag 10:1	21.4	9.7	46.1	13.9	8.1	6	0.453
Ce:Ag 20:1	23.9	4.5	43.8	15.7	7.1	5	0.188
Ce:Ag 30:1	26.6	2.0	39.9	17.4	5.7	3.6	0.075
Ag_2O	–	56	27.3	14.2	0.5	3	–
CeO_2	25.9	–	52.9	21.5	–	–	–

High resolution spectra of the Ag 3d peaks of Ag_2O and Ag doped CeO_2 thin films with the nominal ratio Ce:Ag from 30:1 to 10:1 give us indications of the chemical state of Ag atoms (Figure 11). The pure Ag_2O films showed only one peak at 368.2 eV. The binding energy which has been observed for pure Ag_2O thin film is 367.2 eV, which consists of the dominant oxidation state Ag^+ [33]. The spectrum here shows a shift of ~1 eV in the peak position compared to the previously found results which may be due to sample charging. The spectrum showed core level binding energies at about 368.2 ± 0.1 eV and 374.2 ± 0.1 eV related to the Ag $3d_{5/2}$ and Ag $3d_{3/2}$ respectively with spin orbit separation of 6 eV [34]. Each Ag 3d level in Ag doped CeO_2 films can be deconvoluted into three peaks, with corresponding binding energies 368.2, 369.2, and 367.2 eV, which are consistent with those of Ag^+ , Ag^0 , and Ag^{2+} (Table 3), allowing for the shift due to sample charging [35–37]. The estimated percentages of the three peaks, shown in Table 3, indicates that with increasing Ag doping concentration in CeO_2 films from 30:1 to 10:1, the Ag^+ oxidation state also grows from 38.4% to 85%, respectively. At the same time the Ag^0 oxidation state decreases from 59% to 9.7% for CeO_2 doped Ag films deposited with the ratio Ce:Ag from 30:1 to 10:1, respectively.

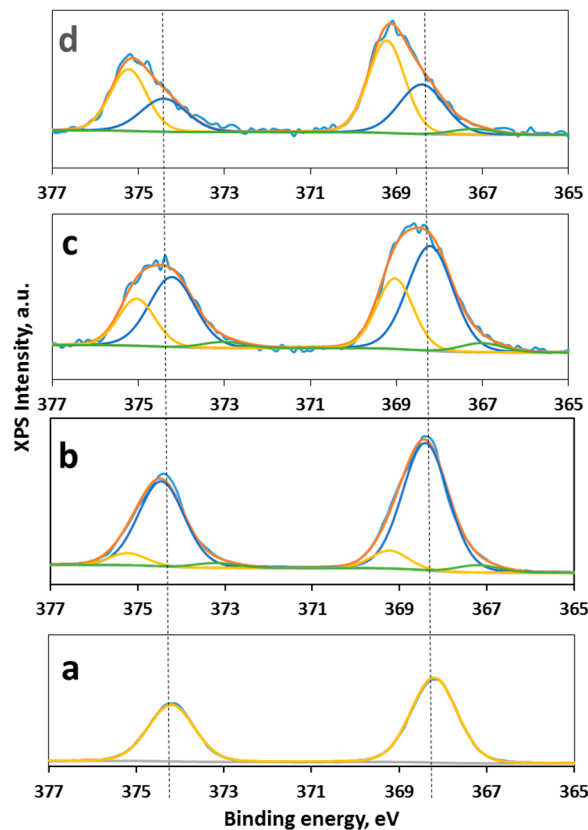


Figure 11. High resolution Ag 3d X-ray photoelectron spectroscopy (XPS) spectra of (a) pure Ag₂O and Ag doped CeO₂ in different CeO₂:Ag ratio (b) 10:1, (c) 20:1, and (d) 30:1.

Table 3. Binding energies and integrated peak areas of Ag 3d spin-orbit doublets in Ag₂O, Ag doped CeO₂ and CeO₂ thin films.

Catalyst	Compound (BE, eV)			Concentration of Ce ⁴⁺ (at.%) (Excluding C)	Concentration of Ce ³⁺ (at.%) (Excluding C)	Ce ³⁺ /Ce ⁴⁺ (%)
	Ag ⁺ (368.2 ± 0.1)	Ag ⁰ (369.2 ± 0.1)	Ag ²⁺ (367.2)			
Ag ₂ O	100	–	–	–	–	–
Ce:Ag 10:1	85	9.7	4.5	77	23	29.8
Ce:Ag 20:1	59	35	6	80	20	25.0
Ce:Ag 30:1	38.4	59	2.6	82	18	21.9
CeO ₂	–	–	–	83	17	20.4

Figure 11 and Table 3 show that at low doping concentration, Ag species mainly exist as Ag⁰, while as doping concentration increases, Ag⁺ species increase remarkably. It is likely that at low concentrations of Ag₂O doping, some of the silver oxide is reduced by the CeO₂; a similar effect has been reported on Ag₂O-doped TiO₂ [38]. For higher Ag dopant concentration, most of the silver present in the catalysts remains as cations and probably interacts with CeO₂ through the Ag–O bonds. Based on previous studies involving silver oxides [39–42], it can be concluded that some electrons may transfer from CeO₂ to the Ag dopant and there is strong interaction between the Ag species and the CeO₂ catalyst.

It is interesting to note that the concentration of Ce⁴⁺ decreased from 82% to 77% and the concentration of Ce³⁺ increased from 18% to 23% with increasing Ce:Ag doping from 30:1 to 10:1, respectively, further suggesting the existence of the interaction between Ag and CeO₂. This is probably because the Ag⁺ ions in Ag doped CeO₂ can partially substitute Ce⁴⁺ in the CeO₂ matrix in the form of Ce_{1-x}Ag_xO_{2-δ}. As was shown earlier from the XRD spectra, there is no evidence of substitutional doping. However, the increasing Ag content also produced smaller crystallites so it may be that the

increasing Ce^{3+} arises as a consequence of interaction between the CeO_2 and the Ag in the disordered regions at the grain boundaries. In summary, Ag atoms deposited on a stoichiometric CeO_2 surface tend to result in reduction of the Ce ions, which leads to the stabilization of the Ag in the +1 oxidation state. These results are in good agreement with the literature reports [43–45].

3.3. Catalytic Activity of Ag_2O , CeO_2 , and Ag-doped CeO_2 catalysts

The evaluation of the catalytic activity of Ag_2O , CeO_2 , and Ag doped CeO_2 thin films deposited at 200 °C on stainless steel foil was carried out to show the effectiveness of the catalysts for soot combustion applications. The annealing tests of carbon soot, which was generated from diesel fuel, was carried out under ambient air environment inside an oven in the temperature range 300–490 °C for 2 h.

Figure 12 shows histograms of soot conversion vs. annealing temperature for catalytic and non-catalytic combustion. The conversion is defined as:

$$C(\%) = \frac{M_0 - M}{M_0} \times 100\% \quad (1)$$

where M_0 is the initial soot mass, and M is the amount of soot left on the catalyst after burning by heating up to a given T value. Weight loss values were obtained by weighing the samples before and after the annealing test which continued for 2 h.

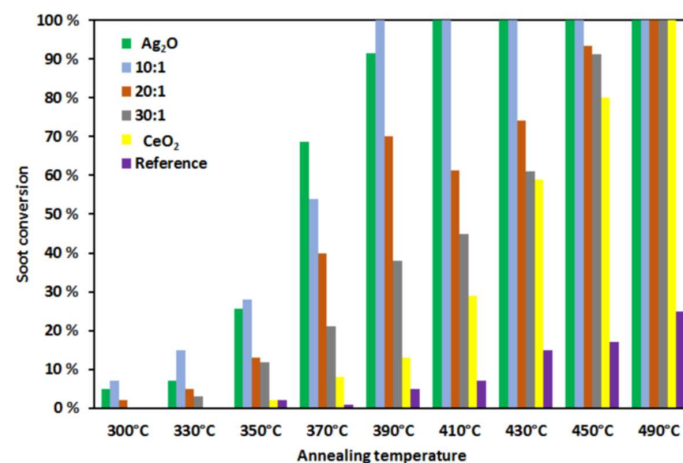


Figure 12. Conversion of oxidized soot on silver oxide, cerium oxide, and silver doped cerium oxide in ratio $CeO_2:Ag$ 10:1, 20:1, 30:1 thin films deposited on stainless steel foil at 200 °C vs. annealing temperature over 2 h. The measurement uncertainty is approximately 5%.

The conversion of oxidized soot was demonstrated on non-catalysed reference steel foil, and on cerium oxide, silver oxide, and Ag doped CeO_2 thin films deposited on stainless steel foil at 200 °C in loose contact mode (Figure 12). As expected, complete soot conversion on the uncoated reference sample was only achieved at 600 °C. All the catalysts were effective in promoting combustion at temperatures below 490 °C. Although the soot was well oxidized on pure CeO_2 and Ag_2O thin films themselves, Ag loading into CeO_2 thin films caused a significant enhancement of soot oxidation rate, in accordance with previous reports [28]. It is noteworthy that the soot oxidation activity of Ag doped CeO_2 was different depending on the dopant concentration. The sample having the maximum silver loading $CeO_2:Ag$ 10:1 and pure Ag_2O showed the lowest oxidation temperature of 300 °C and complete combustion of the soot was achieved below 390 and 410 °C under real-world loose contact conditions, respectively. Table 4 lists the characteristic temperatures, where the ignition temperature (T_i) is the temperature at which the combustion began, and the final temperature (T_f) is the temperature at which the soot was completely oxidized.

Table 4. Catalytic performance for soot oxidation.

Catalyst	T_i (°C)	T_f (°C)
None	410	600
CeO ₂	350	490
CeO ₂ :Ag 10:1	300	390
CeO ₂ :Ag 20:1	300	490
CeO ₂ :Ag 30:1	330	490
Ag ₂ O	300	410

The catalysts with silver doping concentration of Ce₂O:Ag 20:1 and 30:1 showed lower performance for 100% soot oxidation at $T_f = 490$ °C. This indicates that the highest concentration of Ag⁺ ions, which is contained mostly in CeO₂:Ag 10:1 catalyst, can effectively promote 100% soot oxidation at $T_f = 390$ °C due to the oxygen species formed on Ag⁺ sites. Zou et al. [46] proposed that during silver oxide decomposition, its released oxygen migrates to soot surfaces to form carbon–oxygen intermediates, which are subsequently oxidized further. Finally, the adsorbed oxygen on the silver promotes the regeneration process. The redox reaction of Ag⁺ and the active oxygen species prevail in the reaction at low combustion temperatures. In addition, the silver oxide contributes to the adsorption of reactants to form complex π bonds that are significant for the formation of peroxide and superoxide species [47]. It is worth mentioning that higher concentration of Ce³⁺ contained in CeO₂:Ag 10:1 catalyst can also form more active oxygen vacancies, which promote the activation of adsorbed oxygen to form superoxides in the lattice. These types of oxygen react with soot efficiently [48].

Because the melting point of Ag₂O oxides is relatively low, compared with CeO₂ (2400 °C), the stability of Ag/CeO₂ catalysts during the soot oxidation is an important factor from the practical point of view. In order to gain information on the stability of Ag/CeO₂, repetitive activity tests were carried out in loose contact mode at annealing temperature 430 °C. Figure 13 shows the conversion of oxidized soot after five replicate trials, and the observed results showed acceptable reproducibility with relative standard deviation of less than 5%. The pure Ag₂O catalyst lost its catalytic activity immediately after the first trial from 100% to 50% of oxidized soot. Further use of Ag₂O catalyst (in the third, fourth, and fifth trials) led to significant restructuring of the film and total loss of catalytic properties. For this reason, bulk Ag₂O cannot be used in catalytic systems operating at higher temperature (above 300 °C).

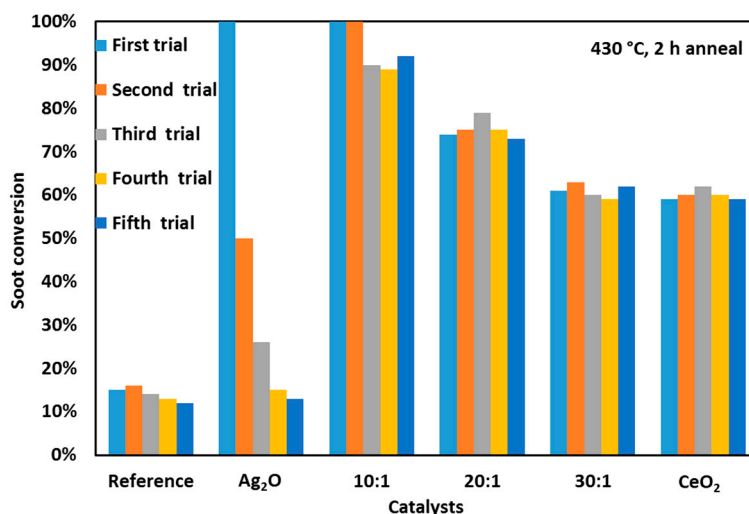


Figure 13. Repetitive soot oxidation in the presence of silver oxide, cerium oxide, and silver doped cerium oxide in ratio CeO₂:Ag 10:1, 20:1, and 30:1 thin films deposited on stainless steel foil at 200 °C vs. annealing temperature over 2 h at 430 °C.

It appears that CeO₂/Ag 10:1 lost 10% of its activity in the third combustion test, indicating the deactivation of Ag/CeO₂. However, during further trials this catalyst showed stable results of 90% oxidized soot. We can assume that Ag ions have a strong interaction with the CeO₂ catalyst and remain stable after durability tests. Other catalysts such as CeO₂:Ag 20:1, 30:1 and pure CeO₂ do not lose activity, since the combustion curves obtained from the first to the fifth tests were very similar.

4. Conclusions

We have demonstrated that ALD can be used to deposit Ag₂O and Ag doped CeO₂ catalysts at 200 °C with (hfac)Ag(PMe₃), Ce(thd)₄ and O₃ as precursors. The growth rate stabilized to a steady-state Ag₂O GPC of 0.28 Å/cycle after 100 ALD cycles. The silver doping concentration was finely tuned by setting the CeO₂:Ag cycle ratio to 10:1, 20:1, and 30:1. With increasing Ag concentration in the CeO₂ thin films, the overall GPC decreased from 0.32 down to 0.21 Å/cycles. AFM and SEM analyses showed that higher concentration of Ag (CeO₂:Ag 10:1) inhibited CeO₂ growth so that the Ag nuclei were not covered with CeO₂ and so the next Ag cycle nucleated more easily on top of the Ag and could therefore form bigger crystals. XRD and XPS analyses showed that the Ag⁺ oxidation state dominated for CeO₂:Ag 10:1 catalysts and stoichiometric CeO₂ tended to be reduced from Ce⁴⁺ to Ce³⁺ ions.

The performance of soot combustion with Ag₂O and Ag doped CeO₂ with different silver concentrations was compared at operating temperatures 300–500 °C. The annealing test showed that higher concentration of Ag⁺ in CeO₂:Ag 10:1 catalytic films was as effective as Ag₂O films; effectively promoting 100% soot oxidation at $T_f = 390$ °C due to the oxygen species formed on Ag⁺ sites. It is worth mentioning that the higher concentrations of Ce³⁺ in the CeO₂:Ag 10:1 catalyst films can also form more active oxygen, which then reacts with soot to yield carbon dioxide.

In repetitive tests in loose contact mode, the Ag doped CeO₂ catalysts showed stable performance after a small initial decrease (down to approximately 90% of the initial performance for the case of CeO₂:Ag 10:1 films) whereas the performance of the pure Ag₂O films decreased by 50% after the first test and continued to decrease thereafter.

Overall, the results show that Ag-doped CeO₂ films grown by ALD are effective and stable as catalysts for soot oxidation.

Author Contributions: Conceptualization, T.V.I. and A.B., D.C.C.; Methodology, T.V.I., T.H., D.C.C.; Investigation, T.V.I., T.H., A.B., D.C.C.; Writing—Original Draft Preparation, T.V. Ivanova, D.C.C.; Supervision, D.C.C.

Funding: This research was funded by TEKES, the Finnish Agency for Technology and Innovation (70006/13), European Regional Development Fund (project CZ.1.05/2.1.00/03.0086), and Ministry of Education Youth and Sports of Czech Republic (project LO1411 (NPU I)).

Acknowledgments: Acknowledgment is given to Monika Stupavská and Pavel Souček for acquiring XPS and XRD data.

Conflicts of Interest: The authors declare no conflict of interest.

References

1. Neeft, J.P.A.; Makkee, M.; Moulijn, J.A. Diesel particulate emission control. *Fuel Process. Technol.* **1996**, *47*, 1–69. [[CrossRef](#)]
2. Nielsen, T.; Jørgensena, H.E.; Larsen, J.C.; Poulsen, M. City air pollution of polycyclic aromatic hydrocarbons and other mutagens: Occurrence, sources and health effects. *Sci. Total Environ.* **1996**, *189–190*, 41–49. [[CrossRef](#)]
3. Anda, A.; Illes, B. Impact of simulated airborne soot on maize growth and development. *J. Environ. Prot.* **2012**, *3*, 773–781. [[CrossRef](#)]
4. Stratakis, G.A.; Stamatelos, A.M. Thermogravimetric analysis of soot emitted by a modern diesel engine run on catalyst-doped fuel. *Combust. Flame* **2003**, *132*, 157–169. [[CrossRef](#)]
5. Jequirim, M.; Tshamber, V.; Brilac, J.F.; Ehrburger, P. Oxidation mechanism of carbon black by NO₂: Effect of water vapour. *Fuel* **2005**, *84*, 1949–1956. [[CrossRef](#)]

6. Pisarello, M.L.; Milt, V.; Peralta, M.A.; Querini, C.A.; Miró, E.E. Simultaneous removal of soot and nitrogen oxides from diesel engine exhausts. *Catal. Today* **2002**, *75*, 465–470. [[CrossRef](#)]
7. Prasad, R.; Bella, V.R. A review on diesel soot emission, its effect and control. *Bull. Chem. React. Eng. Catal.* **2010**, *5*, 69–86. [[CrossRef](#)]
8. Trovarelli, A.; de Lietenborg, C.; Boaro, M.; Dolcetti, G. The utilization of ceria in industrial catalysis. *Catal. Today* **1999**, *50*, 353–367. [[CrossRef](#)]
9. Machida, M.; Murata, Y.; Kishikawa, K.; Zhang, D.; Ikeue, K. On the reasons for high activity of CeO₂ catalyst for soot oxidation. *Chem. Mater.* **2008**, *20*, 4489–4494. [[CrossRef](#)]
10. Oliveira, C.F.; Garcia, F.A.C.; Araujo, D.R.; Macedo, J.L.; Dias, S.C.L.; Dias, J.A. Effects of preparation and structure of cerium-zirconium mixed oxides on diesel soot catalytic combustion. *Appl. Catal. A Gen.* **2012**, *413–414*, 292–300. [[CrossRef](#)]
11. Krishna, K.; Bueno-Lopez, A.; Makkee, M.; Mouljin, J.A. Potential rare earth modified CeO₂ catalysts for soot oxidation: I. Characterisation and catalytic activity with O₂. *Appl. Catal. B Environ.* **2007**, *75*, 189–200. [[CrossRef](#)]
12. Vinodkumar, T.; Rao, B.G.; Reddy, B.M. Influence of isovalent and aliovalent dopants on the reactivity of cerium oxide for catalytic applications. *Catal. Today* **2015**, *253*, 57–64. [[CrossRef](#)]
13. Durgasri, D.N.; Vinodkumar, T.; Lin, F.; Alxneit, I.; Reddy, B.M. Gadolinium doped cerium oxide for soot oxidation: Influence of interfacial metal-support interactions. *Appl. Surf. Sci.* **2014**, *314*, 592–598. [[CrossRef](#)]
14. Bueno-Lopez, A.; Krishna, K.; Makkee, M.; Mouljin, J.A. Enhanced soot oxidation by lattice oxygen via La³⁺-doped CeO₂. *J. Catal.* **2005**, *230*, 237–248. [[CrossRef](#)]
15. Atribak, I.; Bueno-Lopez, A.; Garcia-Garcia, A. Combined removal of diesel soot particulates and NO_x over CeO₂-ZrO₂ mixed oxides. *J. Catal.* **2008**, *259*, 123–132. [[CrossRef](#)]
16. Scire, S.; Riccobene, S.P.M.; Crisafulli, C. Ceria supported group IB metal catalysts for the combustion of volatile organic compounds and the preferential oxidation of CO. *Appl. Catal. B Environ.* **2010**, *101*, 109–117. [[CrossRef](#)]
17. Tarasov, A.L.; Przhevalskaya, L.K.; Shvets, V.A.; Kazanskii, V.B. Influence of the metal-oxide electronic interaction on the reactivity of adsorbed oxygen radicals. Applied catalysts containing cerium oxide and Cu, Ag, and Au. *Kinet. Katal.* **1988**, *29*, 1181–1188.
18. Soria, J.; Martinez-Arias, A.; Conesa, J.C. Effect of oxidized rhodium on oxygen adsorption on cerium oxide. *Vacuum* **1992**, *43*, 437–440. [[CrossRef](#)]
19. Rangaswamy, A.; Sudarsanam, P.; Reddy, B.M. Rare earth metal doped CeO₂-based catalytic materials for diesel soot oxidation at lower temperatures. *J. Rare Earths* **2015**, *33*, 1162–1169. [[CrossRef](#)]
20. Aneggi, E.; Llorca, J.; de Leitenborg, C.; Dolcetti, G.; Trovarelli, A. Soot combustion over silver-supported catalysts. *Appl. Catal. Environ.* **2009**, *91*, 489–498. [[CrossRef](#)]
21. Hanedaa, M.; Towata, A. Catalytic performance of supported Ag nano-particles prepared by liquid phase chemical reduction for soot oxidation. *Catal. Today* **2015**, *242*, 351–356. [[CrossRef](#)]
22. Kuwahara, Y.; Fujibayashi, A.; Uehara, H.; Mori, K.; Yamashita, H. Catalytic combustion of diesel soot over Fe and Ag-doped manganese oxides: Role of heteroatoms in the catalytic performances. *Catal. Sci. Technol.* **2018**, *8*, 1905–1914. [[CrossRef](#)]
23. Shimizu, K.; Kawachi, H.; Satsuma, A. Study of active sites and mechanism for soot oxidation by silver-loaded ceria catalyst. *Appl. Catal. B Environ.* **2010**, *96*, 169–175. [[CrossRef](#)]
24. Preda, G.; Pacchioni, G. Formation of oxygen active species in Ag-modified CeO₂ catalyst for soot oxidation: A DFT study. *Catal. Today* **2011**, *177*, 31–38. [[CrossRef](#)]
25. Yamazaki, K.; Kayama, T.; Dong, F.; Shinjoh, H. A mechanistic study on soot oxidation over CeO₂-Ag catalyst with ‘rice-ball’ morphology. *J. Catal.* **2011**, *282*, 289–298. [[CrossRef](#)]
26. Castoldi, L.; Aneggi, E.; Matarrese, R.; Bonzi, R.; Llorca, J.; Trovarelli, A.; Lietti, L. Silver-based catalytic materials for the simultaneous removal of soot and NO_x. *Catal. Today* **2015**, *258*, 405–415. [[CrossRef](#)]
27. O’Neill, B.J.; Jackson, D.H.K.; Lee, J.; Canlas, C.; Stair, P.C.; Marshall, C.L.; Elam, J.W.; Kuech, T.F.; Dumesic, J.A.; Huber, G.W. Catalyst design with atomic layer deposition. *ACS Catal.* **2015**, *5*, 1804–1825. [[CrossRef](#)]
28. Ivanova, T.V.; Toivonen, J.; Homola, T.; Maydannik, P.S.; Kääriäinen, T.; Sillanpää, M.; Cameron, D.C. Atomic layer deposition of cerium oxide for potential use in diesel soot combustion. *J. Vac. Sci. Technol. A* **2016**, *34*, 031506. [[CrossRef](#)]

29. Masango, S.S.; Peng, L.; Marks, L.D.; Van Duyne, R.P.; Stair, P.C. Nucleation and growth of silver nanoparticles by AB and ABC-type atomic layer deposition. *J. Phys. Chem. C* **2014**, *118*, 17655–17661. [[CrossRef](#)]
30. Puurunen, R.; Vandervorst, W. Island growth as a growth mode in atomic layer deposition: A phenomenological model. *J. Appl. Phys.* **2004**, *96*, 7686. [[CrossRef](#)]
31. Shannon, R.D. Revised effective ionic radii and systematic studies of interatomic distances in halides and chalcogenides. *Acta Crystallogr. A* **1976**, *32*, 751–767. [[CrossRef](#)]
32. Cui, X.S. *The Basic Theory of Solid Chemistry*; Beijing Institute of Technology Printing: Beijing, China, 1991. (In Chinese)
33. Murray, B.J.; Li, Q.; Newberg, J.T.; Menke, E.J.; Hemminger, J.C.; Penner, R.M. Shape- and size-selective electrochemical synthesis of dispersed silver(I) oxide colloids. *Nano Lett.* **2005**, *5*, 2319–2324. [[CrossRef](#)] [[PubMed](#)]
34. Tjeng, L.H.; Meinders, M.B.J.; van Elp, J.; Ghijsen, J.; Sawatzky, G.A.; Johnson, R.L. Electronic structure of Ag₂O. *Phys. Rev. B* **1990**, *41*, 3190–3194. [[CrossRef](#)]
35. Abe, Y.; Hasegawa, T.; Kawamura, M.; Sasaki, K. Characterization of Ag oxide thin films prepared by reactive RF sputtering. *Vacuum* **2004**, *76*, 1–6. [[CrossRef](#)]
36. Kaspar, T.C.; Droubay, T.; Chambers, S.A.; Bagus, P.S. Spectroscopic evidence for Ag(III) in highly oxidized silver films by X-ray photoelectron spectroscopy. *J. Phys. Chem. C* **2010**, *114*, 21562–21571. [[CrossRef](#)]
37. Ferraria, A.M.; Carapeto, A.P.; do Rego, A.M.B. X-ray photoelectron spectroscopy: Silver salts revisited. *Vacuum* **2012**, *86*, 1988–1991. [[CrossRef](#)]
38. Sadanandam, G.; Kumari, V.D.; Scurrrell, M.S. Highly stabilized Ag₂O-loaded nano TiO₂ for hydrogen production from glycerol: Water mixtures under solar light irradiation. *Int. J. Hydrogen Energy* **2017**, *42*, 807–820. [[CrossRef](#)]
39. Zhang, H.; Wang, G.; Chen, D.; Lv, X.; Li, J. Tuning photoelectrochemical performances of Ag-TiO₂ nanocomposites via reduction/oxidation of Ag. *Chem. Mater.* **2008**, *20*, 6543–6549. [[CrossRef](#)]
40. Xin, B.; Jing, L.; Ren, Z.; Wang, B.; Fu, H. Effects of simultaneously doped and deposited Ag on the photocatalytic activity and surface states of TiO₂. *J. Phys. Chem.* **2005**, *109*, 2805–2809. [[CrossRef](#)] [[PubMed](#)]
41. Priya, K.V.B.R.; Shukla, S.; Biju, S.; Reddy, M.L.P.; Patil, K.; Warriar, K.G.K. Comparing ultraviolet and chemical reduction techniques for enhancing photocatalytic activity of silver oxide/silver deposited nanocrystalline anatase titania. *J. Phys. Chem. C* **2009**, *113*, 6243–6255. [[CrossRef](#)]
42. Li, J.; Xu, J.; Dai, W.-L.; Fan, K. Dependence of Ag deposition methods on the photocatalytic activity and surface state of TiO₂ with twistlike helix structure. *J. Phys. Chem. C* **2009**, *113*, 8343–8349. [[CrossRef](#)]
43. Ansari, A.A.; Labis, J.P.; Alam, M.; Ramay, S.M.; Ahmed, N.; Mahmood, A. Preparation and spectroscopic, microscopic, thermogravimetric, and electrochemical characterization of silver-doped cerium(IV) oxide nanoparticles. *Anal. Lett.* **2017**, *50*, 1360–1371. [[CrossRef](#)]
44. Deshpande, S.S.; Patil, S.V.N.; Kuchibhatla, T.; Seal, S. Size dependency variation in lattice parameter and valency states in nanocrystalline cerium oxide. *Appl. Phys. Lett.* **2005**, *87*, 133113. [[CrossRef](#)]
45. Cai, S.; Zhang, D.; Zhang, L.; Huang, L.; Li, H.; Gao, R.; Shi, L.; Zhang, J. Comparative study of 3D ordered macroporous Ce_{0.75}Zr_{0.2}M_{0.05}O_{2-δ} (M = Fe, Cu, Mn, Co) for selective catalytic reduction of NO with NH₃. *Catal. Sci. Technol.* **2014**, *4*, 93–101. [[CrossRef](#)]
46. Zou, G.; Fan, Z.; Yao, X.; Zhang, Y.; Zhang, Z.; Chen, M.; Shangguan, W. Catalytic performance of Ag/Co-Ce composite oxides during soot combustion in O₂ and NO_x: Insights into the effects of silver. *Chin. J. Catal.* **2017**, *38*, 564–572. [[CrossRef](#)]
47. Bukhtiyarov, V.I.; Havecker, M.; Kaichev, V.V.; Knop-Gericke, A.; Mayer, R.W.; Schlögl, R. Atomic oxygen species on silver: Photoelectron spectroscopy and X-ray absorption studies. *Phys. Rev. B* **2003**, *67*, 235422. [[CrossRef](#)]
48. Aneggi, E.; de Leitenburg, C.; Llorca, J.; Trovarelli, A. Higher activity of diesel soot oxidation over polycrystalline ceria and ceria–zirconia solid solutions from more reactive surface planes. *Catal. Today* **2012**, *197*, 119–126. [[CrossRef](#)]

